Solid State Ionics 296 (2016) 63–70

Contents lists available at ScienceDirect

Solid State Ionics

journal homepage: www.elsevier.com/locate/ssi

Crystallization of amorphous $Na_2Si_2O_5$ as a Na-ion conductor

Youngseok Jee [a], Po-Hsiu Chien [b], Esteban Villarreal [c], Yan-Yan Hu [b], Kevin Huang [a,*]

[a] Department of Mechanical Engineering, University of South Carolina, Columbia, SC 29201, USA
[b] Department of Chemistry and Biochemistry, Florida State University, Tallahassee, FL 32306, USA
[c] Department of Chemistry, University of South Carolina, Columbia, SC 29201, USA

ARTICLE INFO

Article history:
Received 28 May 2016
Received in revised form 2 July 2016
Accepted 5 September 2016
Available online 11 September 2016

Keywords:
Electrochemical cell
Na^+ conductor
Conductivity
Amorphous
Crystallization

ABSTRACT

The $Na_2Si_2O_5$ in the amorphous state exhibits a fast Na^+-conduction at elevated temperatures. However, it is metastable, gradually transforming into the insulating $Na_2Si_2O_5$ in the crystalline state with temperatures. The present work shows that the presence of H_2 and Al-doping can suppress the harmful amorphous-to-crystalline transformation in $Na_2Si_2O_5$. A systematic investigation was carried out to understand the fundamental aspects of the amorphous-to-crystalline transformation through a suite of advanced experimental techniques including X-ray diffraction (XRD), differential scanning calorimetry (DSC) analysis, electrochemical impedance spectroscopy (EIS), Raman spectroscopy and multi-nucleus nuclear magnetic resonance spectroscopy (NMR).

1. Introduction

Solid-state fast-ion conductors are a class of highly pursued materials for energy-efficient and environmentally clean electrochemical energy conversion and storage devices such as batteries, fuel cells and gas separation membranes. The mobile ions in solid crystalline fast-ion conductors developed in the past include F^- in PbF_2 [1–3], Ag^+ in AgI [4–6], Na^+ in β''-Al_2O_3 [7–8], Li^+ in $Li_5La_3M_2O_{12}$ (M = Nb, Ta) [9–10] and O^{2-} in Y-doped ZrO_2 [11], just to name a few.

Recently, the amorphous $Na_2Si_2O_5$ exhibiting an ionic conductivity of 0.01 S/cm^2 at 500 °C has also been identified as a Na^+-conductor. [12,13] A further study of this material revealed that the amorphous $Na_2Si_2O_5$ phase was unstable at elevated temperatures, transforming into a poorly conducting crystalline phase of the same composition and leading to a fast degradation of conductivity [14,15]. How to retain the conducting amorphous phase and thus a high ionic conductivity becomes a key for this material to be practically meaningful.

In the present study, we investigate the factors affecting the crystallization process of the amorphous $Na_2Si_2O_5$ such as atmosphere and doping. Conventional techniques such as electrochemical impedance spectroscopy (EIS), differential scanning calorimetry (DSC), X-ray diffraction (XRD), Raman Spectroscopy and Nuclear Magnetic Resonance (NMR) Spectroscopy were particularly employed to characterize electrical, chemical and thermal properties of the undoped and Al-doped amorphous $Na_2Si_2O_5$ exposed to a broad range of atmospheres.

2. Experimental procedures

2.1. Sample preparation

Na_2CO_3 (99.9%; Fisher Scientific Inc., Hampton, NH), and SiO_2 (99.9%; Alfa Aesar, Ward Hill, MA) were used as the raw materials to prepare the amorphous $Na_2Si_2O_5$. The powders with the molar ratio of 1:2 were mixed for 20 min in a high-energy mechanical mixer (8000 M Mixer/Mill®; SPEX®; SamplePrep LLC, Metuchen, NJ) in the presence of alcohol and ZrO_2 milling balls. The well-mixed powders were then dried and then pelletized under 5 MPa, followed by calcination at 800 °C for 10 h. Thus pre-calcined pellets were then broken into fine particles of 1–2 μm with a high-energy vibrational mill (Micronizing Mill; The McCrone Group Inc., Westmont, IL). The samples were finally sintered at 900 °C for 10 h in an alumina crucible with a slow heating rate of 2 °C/min, followed by quenching to room temperature. Since the melting temperature of the material is 848.8 °C, [15] lower than 900 °C, the samples were fully melted and transparent.

To study the effect of dopant on the crystallization process, only 5 mol% alumina added $Na_2Si_2O_5$ was prepared from raw Na_2CO_3, SiO_2 and alpha phase alumina (α-Al_2O_3, >99%; Sigma-Aldrich, St. Louis, MO) with the atomic ratio of 100:95:5 (Na:Si:Al). Except the raw materials, the preparation steps for the doped sample were identical to the undoped sample. For the sake of convenience, we labeled the two samples as AM-$Na_2Si_2O_5$ for the amorphous $Na_2Si_2O_5$ and AL-$Na_2Si_2O_5$ for the alumina-doped one.

To study the atmosphere effect, the prepared AM-$Na_2Si_2O_5$ and AL-$Na_2Si_2O_5$ were treated at 500 °C for 100 h in pure H_2 or in air. The

* Corresponding author.
E-mail address: huang46@cec.sc.edu (K. Huang).

http://dx.doi.org/10.1016/j.ssi.2016.09.005
0167-2738/

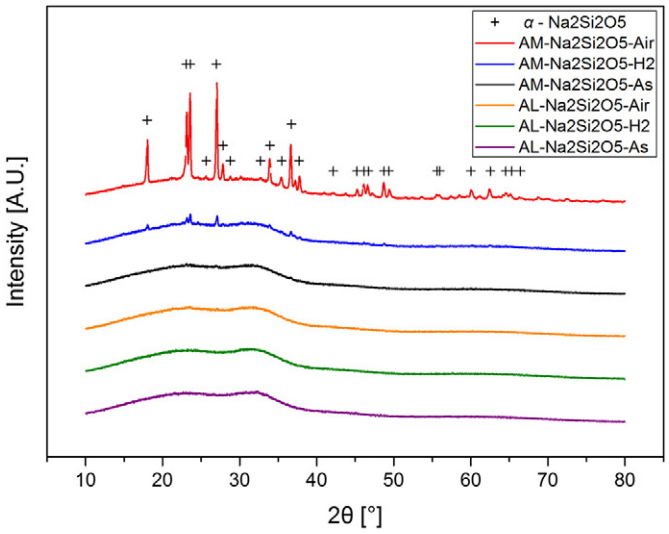

Fig. 1. XRD patterns of as-prepared and H_2/air-treated (at 500 °C for 100 h) AM-$Na_2Si_2O_5$ and AL-$Na_2Si_2O_5$.

samples prepared were subject to characterizations of XRD, Raman spectroscopy and NMR.

2.2. X-ray diffraction

The phase compositions of the samples prepared were examined at room temperature with a powder X-ray diffractometer (D/Max-2100; Rigaku Corporation, Tokyo, Japan) and CuKa radiation (k = 1.5418 Å). The scan was performed in the range of 2θ = 10–80° at a rate of 1° per min and in a step size of 0.04°. The spectra collected were carefully analyzed with JADE (Materials Data Inc., Livermore, CA) to identify phase compositions.

2.3. Electrical conductivity measurement

The electrical conductivity of all the samples was evaluated by electrochemical impedance spectroscopy (EIS). A typical EIS symmetrical cell consisted of a 2-mm thick pellet with a pair of identical screen printed electrode/current collector made of silver paste (C8829; Heraeus Holding GmbH, Hanau, Germany) and mesh (40935, Alfa Aesar). The EIS spectra were collected with an electrochemical station (1260/1287; Solartron Analytical, Farnborough, UK) in the air as well as in H_2 gas flowed at 50 sccm in the temperature range of 200–700 °C. At each temperature, a 10- min stabilization time was given before measurement. The frequency was swept in the range of 0.5 Hz–1 MHz with an AC stimulus voltage of 50 mV. For conductivity *vs* atmosphere study, the spectra were collected as a function of time at 500 °C. The gases investigated include 100% O_2, air, 1% O_2-N_2, 0.1% O_2-N_2, 5% H_2-N_2, 100% H_2, 12% AH humidified H_2 and 31% AH humidified H_2. The humidity was controlled by a water bubbler.

2.4. Thermal analysis

To understand the crystallization process, differential scanning calorimetry (DSC) was carried out with a thermal analyzer (STA 449F1; Netzsch Group, Selb, Germany) in the temperature range of RT–900 °C at a heating/cooling rate of 5 °C/min in a flowing air and 4% H_2-N_2 at 20 mL/min.

2.5. Raman spectroscopy

SERS (Surface-enhanced Raman spectroscopy) spectra were collected from a nomadic confocal Raman Microscope (Bayspec Inc., San Jose, CA) built on a BX51 reflected optical system (Olympus, Tokyo, Japan) with a 785 nm continuous wave excitation laser. Excitation laser was focused on sample with a 10× objective (Numerical Aperture (NA) = 0.30, working distance (WD) = 11.0 mm, Olympus MPLFLN). Laser power was measured to be 10 mW at samples and integration time was 10 s.

2.6. Solid-state NMR characterization

A rotor-synchronized spin-echo pulse sequence was employed for all the experiments with corresponding pulse lengths and recycle delays detailed in the following for each type of nucleus.

The ^{1}H NMR spectra were recorded at the Larmor frequency of 300 MHz with a Bruker DRX-300 spectrometer (Bruker Corporation, Billerica, MA) using a Bruker 4-mm MAS (magic angle spinning) probe spinning at 10 kHz. The π/2 pulse length is 5.65 μs and the recycle delay is 1 s. The ^{1}H NMR shifts were referenced to TMS at 0 ppm for all samples. Due to a strong interference from the background signals, all ^{1}H spectra were subtracted from the background spectrum collected by following the same procedure as mentioned above with an empty rotor spinning at 10 kHz.

The ^{29}Si NMR spectra were collected at the Larmor frequency of 59.6 MHz with a Bruker DRX-300 spectrometer using a Bruker 4-mm MAS probe spinning at 10 kHz. The π/2 pulse length is 4.5 μs and the recycle delay is 2 s. The ^{29}Si NMR shifts were referenced to 4,4-dimethyl-4-silapentane-1-sulfonic acid at 0 ppm.

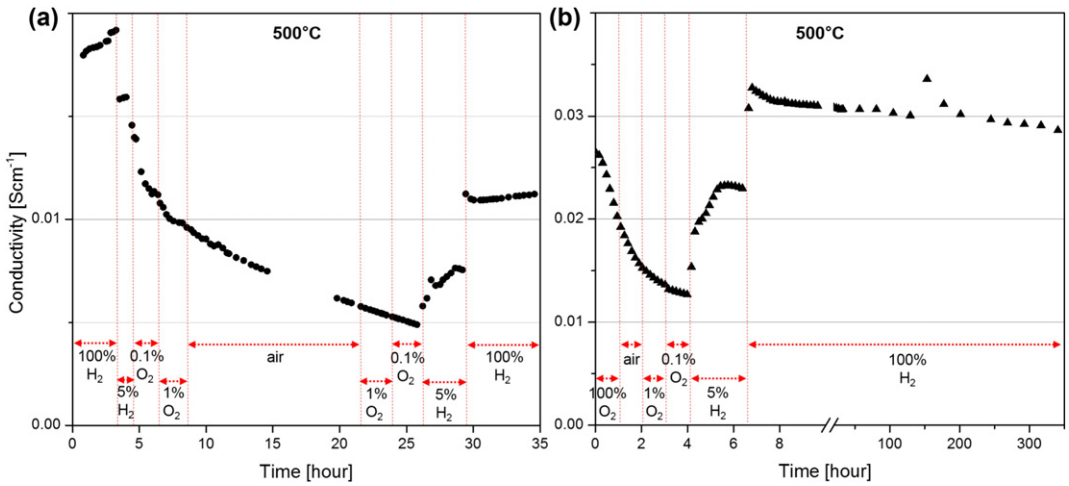

Fig. 2. Conductivity evolution of (a) AM-$Na_2Si_2O_5$ and (b) AL-$Na_2Si_2O_5$ under different atmospheres at 500 °C.

The ^{27}Al NMR spectra were recorded at the Larmor frequency of 78.2 MHz with a Bruker DRX-300 spectrometer using a Bruker 4-mm MAS probe spinning at 10 kHz. The π/2 pulse length is 1.5 μs and the recycle delay is 0.1 s. The ^{27}Al NMR shifts were referenced to 1 M $Al(NO_3)_3$ solution at 0 ppm.

All the ^{23}Na and ^{17}O NMR spectra were acquired on a Bruker DRX-830 spectrometer to achieve high resolution and high sensitivity. All ^{23}Na NMR spectra were recorded at the Larmor frequency of 219.6 MHz with a home-built 1.8-mm MAS probe spinning at 20 kHz. The π/2 pulse length is 3 μs and the recycle delay is 2 s. The ^{23}Na shifts were referenced to 1 M NaCl solution at 0 ppm. All ^{17}O NMR spectra were recorded at the Larmor frequency of 112.6 MHz with a home-built low-E and high-sensitivity 3.2-mm MAS probe [16] spinning at 15 kHz. The π/2 pulse length is 1.08 μs and the recycle delay is 0.1 s. All the ^{17}O shifts were referenced to H_2O at 0 ppm.

Simulations and spectral analysis of all the NMR spectra were carried out using the Topspin (v3.2) software.

3. Results and discussion

3.1. XRD patterns

Fig. 1 shows XRD patterns of as-prepared $Na_2Si_2O_5$ (doped and undoped) as well as those treated in air and H_2 for 100 h. It is evident that the as-prepared original sample (black) indicates an amorphous phase. After exposing to H_2 at 500 °C for 100 h, the undoped sample (blue curve) begins to show very small crystalline peaks but still with a majority of amorphous composition similar to the as-prepared one. In contrast, the air-treated sample (red) shows a significant amount of crystalline phase, which is consistent with our early reports [14,15]. The comparison between samples annealed in H_2 and air suggests that reducing atmosphere can alleviate the crystallization process.

Different from the undoped AM-$Na_2Si_2O_5$ samples, the Al-doped AL-$Na_2Si_2O_5$ show a consistent amorphous phase composition regardless of heat-treatment conditions (see purple, green and orange curves in Fig. 1), which suggests that the presence of Al in the AM-$Na_2Si_2O_5$ can effectively suppress the crystallization process. Because of the suppressed crystallization, we expect that the conductivity degradation of these Al-doped samples will be less than the undoped ones. The same is true for the conductivity in reducing atmospheres.

3.2. Conductivity vs atmosphere

The electrical conductivity of AM-$Na_2Si_2O_5$ and AL-$Na_2Si_2O_5$ under different atmospheres is shown in Fig. 2 on a continuous time scale. After the temperature stabilization in the air for 30 min, AM-$Na_2Si_2O_5$ measurement was started in pure H_2 where conductivity is high and grows with time. After switching to 5%H_2-N_2 at 3 h marker, the level of conductivity is reduced, but still with a rising trend. However, as soon as an O_2-containing atmosphere was introduced during 4 to 26 h, the degradation of conductivity is observed. The degradation rate seems independent of the partial pressure of oxygen (0.1% O_2 to 21% O_2) during this period. Over the 22 h period, the conductivity is decreased by ~3×. Interestingly, at >26 h when H_2-containing atmosphere was re-introduced, the conductivity is increased again with the magnitude increasing with the H_2-content in the atmosphere. The final conductivity in pure H_2 is ~2× the value in oxidizing atmospheres, but only one half the original one.

Fig. 2(b) shows the conductivity of the Al-doped AL-$Na_2Si_2O_5$. The measurement was started in pure O_2 for this sample. The trend that conductivity degradation in oxidizing atmospheres during the first 4 h remains. Upon switching to H_2-containing gases, the conductivity sharply increases and holds a higher value with a slight decline for the

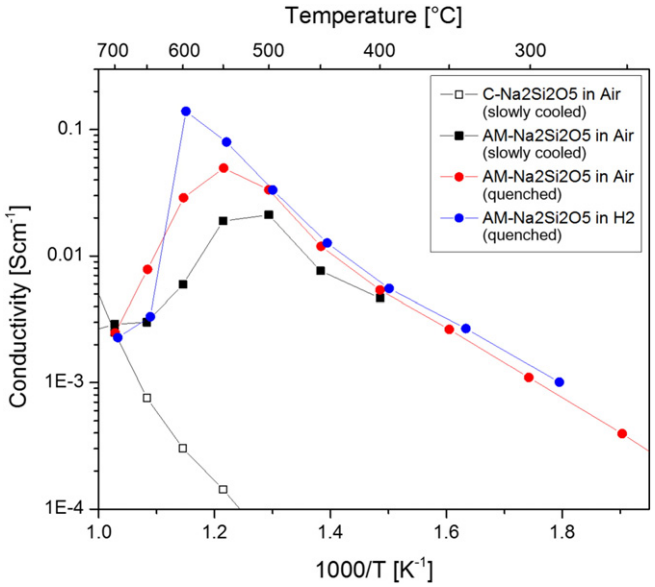

Fig. 4. Conductivity Arrhenius plot of AM-$Na_2Si_2O_5$ fabricated under different conditions.

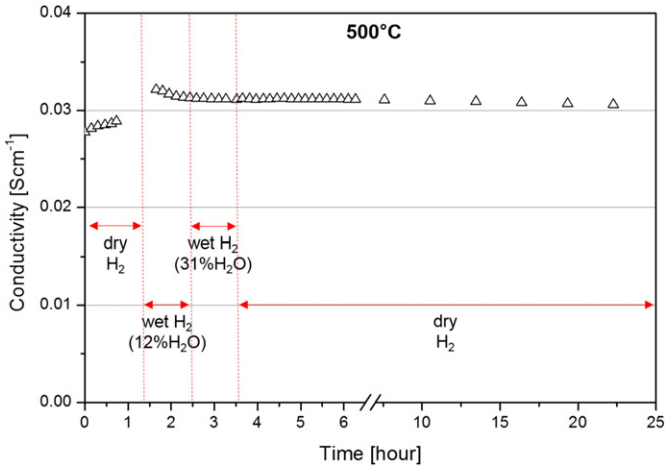

Fig. 3. The conductivity *vs* H_2O concentration of AL-$Na_2Si_2O_5$ at 500 °C.

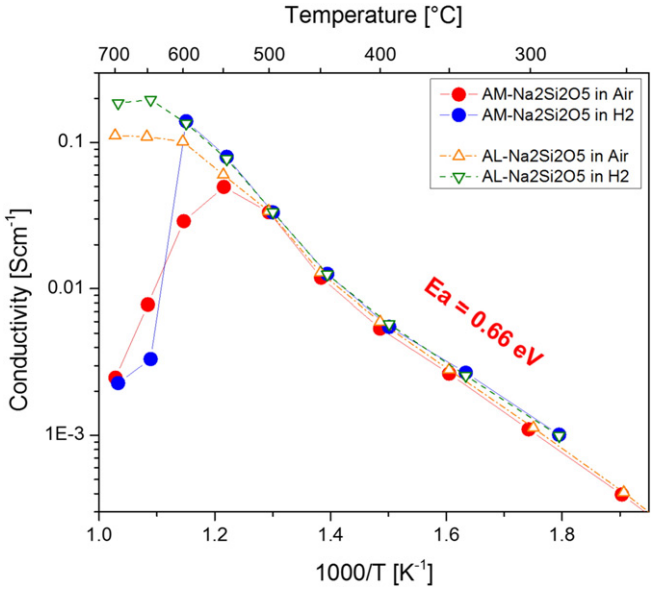

Fig. 5. Conductivity comparison between AM-$Na_2Si_2O_5$ and AL-$Na_2Si_2O_5$ in air and H_2.

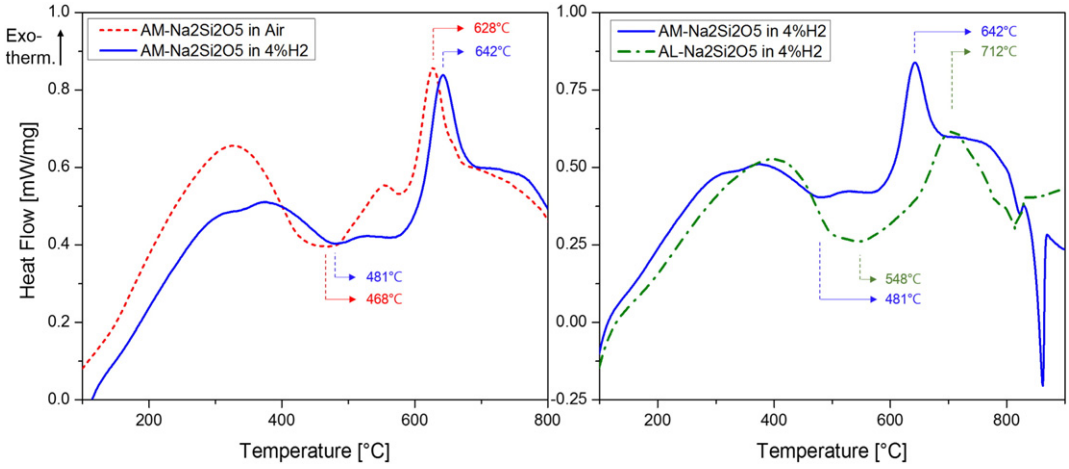

Fig. 6. Comparison of DSC profiles for (a) AM-$Na_2Si_2O_5$ in air *vs* 4% H_2-N_2 and (b) AL-$Na_2Si_2O_5$ *vs* AM-$Na_2Si_2O_5$ in 4% H_2-N_2.

next 350 h. Overall, the level of conductivity of AL-$Na_2Si_2O_5$ is generally higher than AM-$Na_2Si_2O_5$ for a given atmosphere.

The conductivity results shown in Fig. 2 are consistent with the phase evolution revealed by the XRD results in Fig. 1. In the oxidizing atmospheres, the rising concentration of less conducting crystalline phase results in conductivity degradation to lower values, whereas in the reducing atmospheres, the suppressed crystalline phase helps retain the high conductivity present in the AM-$Na_2Si_2O_5$. The electronic conduction is not the reason for the enhanced conductivity observed in H_2. Later characterization also supports this assertion.

For the AL-$Na_2Si_2O_5$, the generally higher conductivity value is the result of less crystalline-phase in the sample, even though 5 mol% Al may still not be sufficient to completely protect the preferred amorphous phase from being crystallized. The lack of crystalline peaks in Fig. 1 for AL-$Na_2Si_2O_5$ samples after being exposed to all atmospheres could be misleading if the amount of crystalline phase in the sample is well below the detection limit of XRD.

3.3. Conductivity vs humidity

To understand if the observed conductivty jump in H_2-containing atmopsheres is also associated with protons produced from the oxygen lattice *via* the Grotthuss mechanism, we measured conductivity of AL-$Na_2Si_2O_5$ in both dry and wet H_2. The results are shown in Fig. 3, where the conductivity in dry H_2 increases at the beginning, just like the AM-$Na_2Si_2O_5$ case shown in Fig. 2(a). After a 12% H_2O was introduced to dry H_2, the conductivity showed a slight decrease and but quickly stabilized at 0.031 S/cm. A further increase in H_2O concentration to 31% did not change the conductivity. Re-exposing dry H_2 did not have any effect on the conductivity either for the next 19 h. Therefore, it can be concluded the conductivity of AL-$Na_2Si_2O_5$ is independent of the humidity. Considering the fact that one of the representative proton conducting ceramics (Y-doped $BaZrO_3$ or BZY) shows the apparent conductivity difference in dry/wet H_2 atmospheres [17], Grotthuss-type proton conduction is not the cause for the conductivity change observed in H_2. Furthermore, the fact that the proton conducting BZY exhibits different activation energies in air and H_2 [18], whereas both AM-$Na_2Si_2O_5$ and AL-$Na_2Si_2O_5$ show the same activation energy (see Fig. 5), also supports non-proton conduction in AM/AL-$Na_2Si_2O_5$.

3.4. Conductivity vs temperature

Recalling the reason for conductivity degradation, we could infer that H_2 inhibits the crystallization or slows it down at least. The

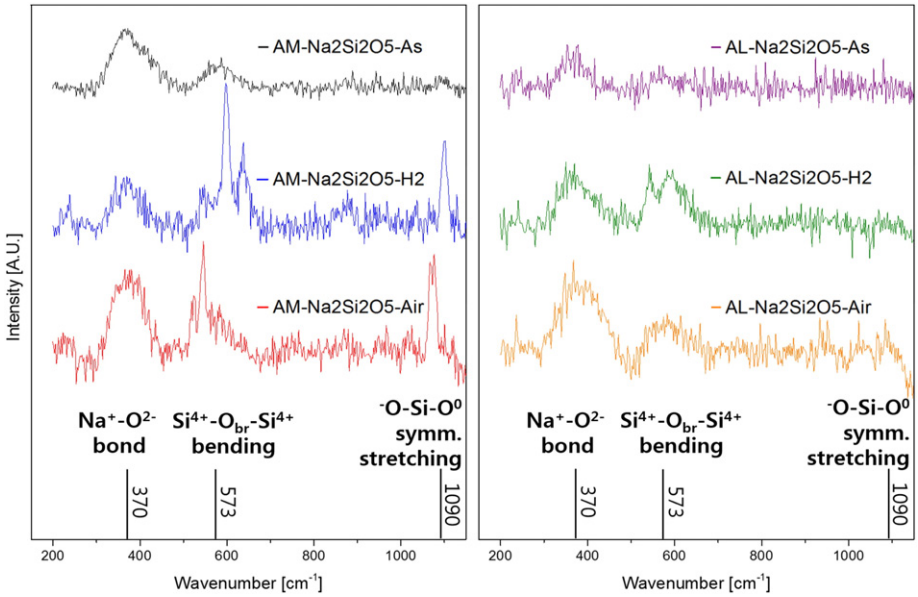

Fig. 7. Raman spectroscopy results on AM/AL-$Na_2Si_2O_5$ treated in various environments.

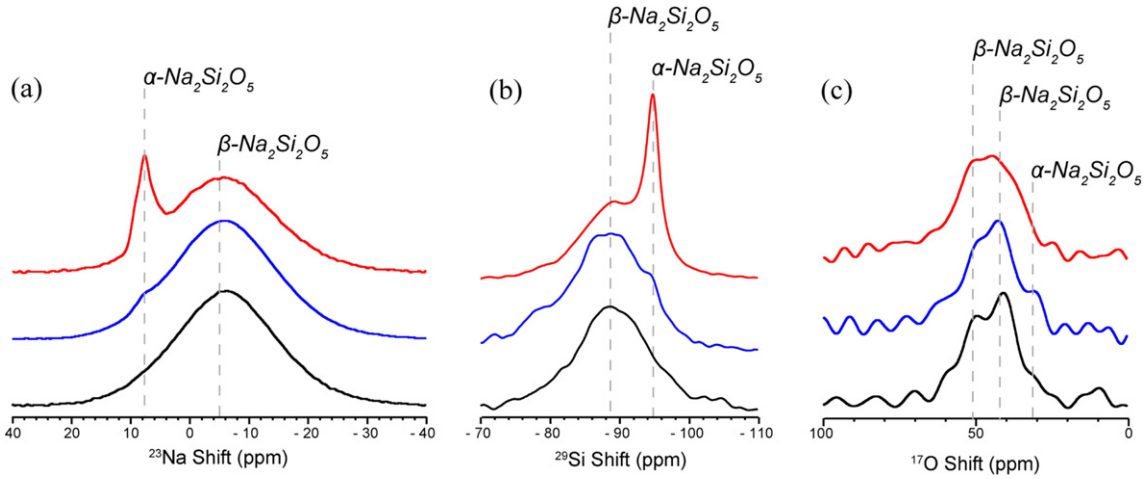

Fig. 8. (a) ^{23}Na, (b) ^{29}Si and (c) ^{17}O MAS NMR spectra of AM-$Na_2Si_2O_5$ as sintered (black), treated in H_2 (blue) and air (red).

conductivity "bend-over" temperature for the "slowly cooled" AM-$Na_2Si_2O_5$ is ~500 °C, and it is increase to ~550 °C for the "quenched" sample, which contains more amorphous phase. The blue data points in Fig. 4 represent the collections from the quenched sample in H_2. This "H_2-quenched" AM-$Na_2Si_2O_5$ shows the highest conductivity "bend-over" temperature at ~600 °C among the three samples. The higher amorphous phase content in the "H_2-quenched" AM-$Na_2Si_2O_5$ sample provides a higher resistance to crystallization, thus yielding a higher "bend-over" temperature. Above the "bend-over" temperature, the conductivity at 700 °C of all the samples falls closely to that of a fully crystallized $Na_2Si_2O_5$ (denoted as C-$Na_2Si_2O_5$ in Fig. 4) fabricated at 840 °C, suggesting that nearly all of the AM-$Na_2Si_2O_5$ has been transformed into C-$Na_2Si_2O_5$ at 700 °C.

For the AL-$Na_2Si_2O_5$ samples, Fig. 5 shows that the conductivities in the air and H_2 at 300–500 °C are almost identical to that of AM-$Na_2Si_2O_5$ with an activation energy of ~0.66 eV before the "bend-over", implying that the Na-ion conduction mechanism remains unchanged. It is also noted that the "bend-over" temperature of AL-$Na_2Si_2O_5$ are higher than AM-$Na_2Si_2O_5$ measured under a similar condition, *e.g.* 600 °C *vs* 500 °C in the air, 650 °C *vs* 600 °C in H_2. The suppressed conductivity "bend-over" implies that AL-$Na_2Si_2O_5$ has a higher resistance to the crystallization process, which is consistent with XRD patterns in Fig. 1, as well as time-dependent conductivity in Fig. 2. In addition, the unchanged conductivity in reducing and oxidizing atmospheres is a strong indicative of ionic conduction.

3.5. DSC analysis

To understand further the crystallization of AM-$Na_2Si_2O_5$, DSC analysis was performed, the results of which are shown in Fig. 6. The crystallization for the AM-$Na_2Si_2O_5$ in air starts at 468 °C and peak at 628 °C, which is clearly lower than those in 4%H_2-N_2 atmosphere (starting at 481 °C and peaking at 642 °C). In addition, the DSC results shown in Fig. 6 (b) indicate a suppressed amorphous-to-crystalline transition for the AL-$Na_2Si_2O_5$ samples. In 4%H_2-N_2, the exothermic crystallization starts at 548 °C, ~67 °C higher than AM-$Na_2Si_2O_5$. The peak temperature is also ~70 °C higher (712 °C) with a lower heat flow, signaling a slower crystallization rate. This is consistent with the XRD and conductivity data shown above. It is, therefore, clear that AL-$Na_2Si_2O_5$ has a better resistance to amorphous-to-crystalline transition, promising it to be a

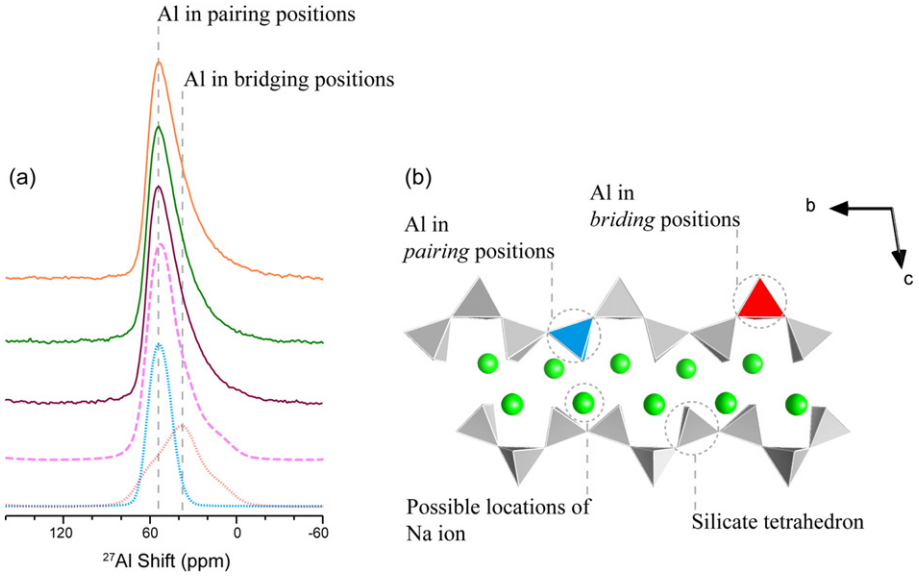

Fig. 9. (a) ^{27}Al MAS NMR spectra of AL-$Na_2Si_2O_5$ treated as sintered (purple), treated in H_2 (green), and air (orange). The simulated spectra are plotted at the bottom in dashed pink line (sum), dotted red line (Al in bridging position), and dotted blue line (Al in pairing position), respectively; (b) schematic presentation of possible locations of Al dopant in the aluminosilicate structure.

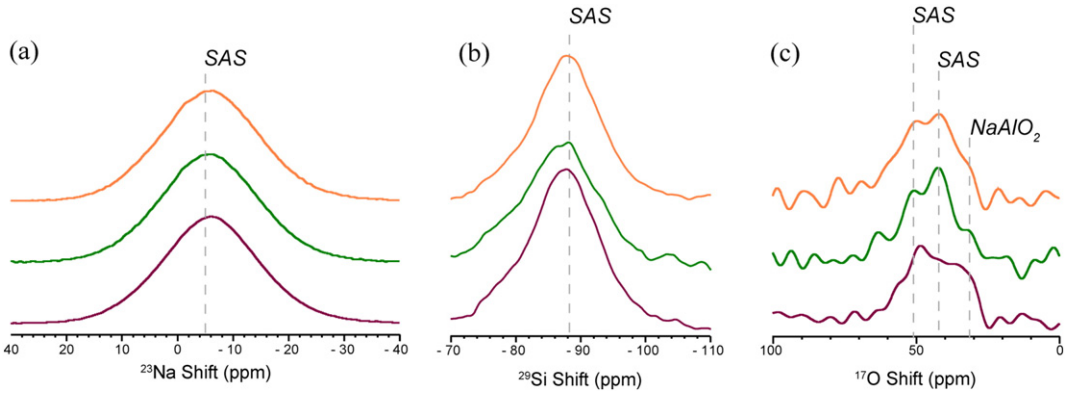

Fig. 10. (a) ^{23}Na, (b) ^{29}Si, and (c) ^{17}O MAS NMR spectra of AL-$Na_2Si_2O_5$ treated as sintered (purple), treated in H_2 (green), and air (orange).

better candidate as an electrolyte for electrochemical cells than the intrinsic AM-$Na_2Si_2O_5$.

3.6. Raman spectroscopy

To understand why and how Al-addition helps suppress the amorphous-to-crystalline transition, Raman spectra were collected at RT; the results are shown in Fig. 7. Crystallographically, $Na_2Si_2O_5$ is consisted of sheets of six-membered rings of SiO_4 tetrahedra and Na-ion is suited between the layers formed by corner-shared Si_2O_5 dimer sheets [19–23]. Fig. 7 shows that all of the six samples investigated exhibit similar features of tetrahedral structure with very similar peak positions. The bands close to 573 cm^{-1} can be assigned to bending vibrations of Si^{4+}-O_{br}-Si^{4+} linkages [24]. For the samples with the crystalline phase (*e.g.* H_2-and air-treated AM-$Na_2Si_2O_5$), the sharper peak near 1090 cm^{-1} is related to $^{-}$O-*Si*-O^0 symmetric stretching [25]. The band near 370 cm^{-1} is due to Na^+ and O^{2-} bonding. However, no structural difference can be discerned for AM-$Na_2Si_2O_5$ and AL-$Na_2Si_2O_5$ samples. Neither are for samples treated in H_2 and air (at 500 °C for 100 h). Therefore, Raman spectroscopy is not a capable technique to identify the root cause of suppressed amorphous-to-crystallization transition.

3.7. Multinuclear (^{29}Si, ^{27}Al, ^{23}Na, ^{17}O and ^{1}H) NMR analyses of AM/AL-$Na_2Si_2O_5$

To have a better understanding of the crystallization process in AM/AL-$Na_2Si_2O_5$, we performed a high-resolution multinuclear solid-state MAS NMR. Each element in AM/AL-$Na_2Si_2O_5$ was probed with its isotope in NMR to gauge the local environment associated with the element of interest.

3.7.1. The local structural environments of AM-$Na_2Si_2O_5$ treated in different atmospheres

The ^{23}Na, ^{29}Si and ^{17}O NMR spectra were acquired to investigate AM-$Na_2Si_2O_5$ treated in different atmospheres. Fig. 8 (a) shows a single broad resonance centered at −5 ppm (the shift is a sum of chemical and quadrupolar shifts) in the ^{23}Na NMR spectrum of AM-$Na_2Si_2O_5$, which is from the amorphous β-$Na_2Si_2O_5$ phase based on our prior studies [26]. A new resonance in the ^{23}Na spectrum is observed at ~8 ppm when amorphous β-$Na_2Si_2O_5$ is heated in air. The well-defined and relatively narrow line shape suggests a crystalline phase, which is identified as α-$Na_2Si_2O_5$ [27]. The appearance of this new resonance indicates a minor phase transformation from amorphous β-$Na_2Si_2O_5$ to crystalline α-$Na_2Si_2O_5$. A significant fraction of the amorphous β-$Na_2Si_2O_5$ phase is converted to crystalline α-$Na_2Si_2O_5$ when it is heated in the air. Consistent observations have been made from ^{29}Si and ^{17}O NMR (Fig. 8(b) and (c)). In ^{29}Si NMR, the sharp resonance of crystalline α-$Na_2Si_2O_5$ appears

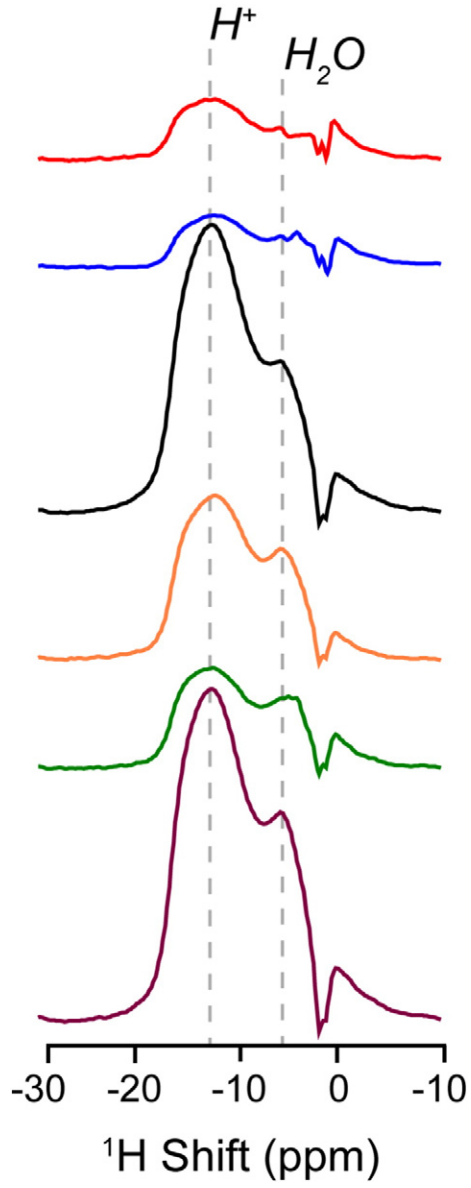

Fig. 11. ^{1}H MAS NMR spectra of AM/AL-$Na_2Si_2O_5$ treated as sintered (black/purple), treated in H_2 (blue/green), and air (red/orange).

at −95 ppm [16], and the broad resonance of amorphous β-$Na_2Si_2O_5$ centers at −88 ppm. Only a small amount of crystalline α-$Na_2Si_2O_5$ is observed in the sample heated in H_2, but a significant increase in the fraction of crystalline α-$Na_2Si_2O_5$ is seen in the sample heated in air. In the ^{17}O NMR (Fig. 8(c)), the resonance of crystalline α-$Na_2Si_2O_5$ shows up as a shoulder to the right of the amorphous β-$Na_2Si_2O_5$ peak [28,29].

In summary, ^{23}Na, ^{29}Si, and ^{17}O NMR spectra of the as-sintered AM-$Na_2Si_2O_5$ and those heated in air and H_2 consistently show that with heat treatment, the presence of O_2 greatly facilitates the conversion of amorphous β-$Na_2Si_2O_5$ to crystalline α-$Na_2Si_2O_5$. The formation of the less conductive crystalline α-$Na_2Si_2O_5$ phase inevitably lowers the ionic conductivity of the material as shown in Figs. 2–5.

3.7.2. The local structural environments of doped-Al

The better stability in both the ionic conductivity (Figs. 2 and 5) and crystallinity (Figs. 1, 6 and 7) at higher temperature is observed for Al-doped AM-$Na_2Si_2O_5$ (AL-$Na_2Si_2O_5$). In order to investigate where the Al dopant ends up in the structure and what leads to the stability, ^{27}Al NMR in addition to ^{23}Na, ^{29}Si, and ^{17}O NMR was acquired and the spectra are presented in Figs. 9 and 10.

The ^{27}Al NMR spectrum of AL-$Na_2Si_2O_5$ in Fig. 9 (a) shows two Al structural environments. Based on the extensive investigation of aluminosilicate reported in the literature [30], Al replaces Si in two different positions, *i.e.* bridging and pairing (Fig. 9(b)), therefore the two ^{27}Al NMR resonances correspond to these two structural sites, with the one at 58 ppm from the paring-Al and the one centering at 38 ppm from bridging-Al. Therefore, the doped Al integrates into the structure to form sodium aluminosilicate (SAS), which is a glassy phase and does not readily crystalize upon heat treatment. The ^{27}Al NMR of AL-$Na_2Si_2O_5$ heated in H_2 or air shows little or no change (Fig. 9(a)). ^{23}Na and ^{29}Si NMR spectra in Fig. 10(a) and (b) confirm that the AL-$Na_2Si_2O_5$ phase stays glassy with heat treatment in H_2 or air. The shoulder on the right of the main AL-$Na_2Si_2O_5$ ^{17}O resonances in the as-sintered AL-$Na_2Si_2O_5$ sample is likely from a minor segregated phase $NaAlO_2$ [31]; further heat treatment in H_2 or air promotes the full integration of $NaAlO_2$ into forming the glassy SAS phase.

In summary, Al integrates into the structure to form the glassy SAS phase, which does not crystalize easily upon heat treatment in either H_2 or air.

3.7.3. Residual H species in AM/AL-$Na_2Si_2O_5$

The ^1H MAS NMR was also acquired to reveal the H species in AM/AL-$Na_2Si_2O_5$ and their changes with heat treatment in H_2 and air. As shown in Fig. 11, the two ^1H resonances are from structural acidic H^+ (13 ppm) and H_2O (5 ppm), respectively. Both species are not expected to be stable at elevated temperatures either in H_2 or in air. Therefore, protons are not a mobile species in AM/AL-$Na_2Si_2O_5$, which is consistent with the results shown in Fig. 3.

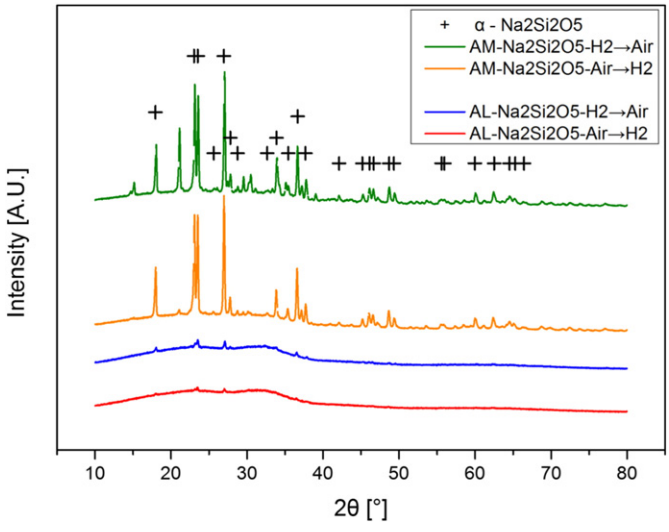

Fig. 12. The crystallinity change in AM-$Na_2Si_2O_5$ and AL-$Na_2Si_2O_5$ samples with atmosphere switch (H_2/air for 100 h → air/H_2 for 500 h at 500 °C).

3.8. Phase reversibility

After 100-h treatment at 500 °C in air, one group of AM-$Na_2Si_2O_5$ and AL-$Na_2Si_2O_5$ samples was re-exposed to 100% H_2 for 500 h. Another group was first heat-treated in 100% H_2 for 100 h, then 500 h in air. Fig. 12 of XRD shows that all the samples exhibit crystalline peaks. The AM-$Na_2Si_2O_5$ sample with H_2 → air or air → H_2 sequence is found to contain a higher content of the crystalline phase than the AL-$Na_2Si_2O_5$. The results suggest that the crystallized phase cannot be fully reversed to the amorphous phase by pure H_2, implying the crystallization is irreversible. While the AL-$Na_2Si_2O_5$ have a better resistance to crystallization, after 500 h heat treatment at 500 °C, a minor degree of crystallization still occurred regardless of atmospheres. In general, an oxidizing environment accelerates the crystallization more than a reducing one.

3.9. A mechanism for H_2-suppressed crystallization

The present study certainly confirms that the presence of H_2 can suppress the crystallization, thus stabilize the conductivity. How H_2 suppresses the crystallization is an interesting scientific question. In the early alloy-based H_2-storage materials research, it was found that RE(rare-earth)-Ni metal alloys tend to be in amorphous state in H_2, resulting in capacity degradation [32,33]. The behavior was explained by a structural perspective that H inserts into slabs and borders of the layered alloy structure and causes anisotropic volume expansion that leads to amorphization [33]. Since $Na_2Si_2O_5$ also has a layered structure [22], it is then reasonable to postulate that H may play a similar role by intercalating into the layers, which inhibits the transition from amorphous to crystalline phase. These hydrogen atoms are not expected to alter the tetrahedral structure of the building units of $Na_2Si_2O_5$. Instead, they may act only as an inhibitor preventing the crystallization.

4. Conclusions

In summary, we observed that the amorphous phase of $Na_2Si_2O_5$ is structurally and electrically more stable in reducing atmospheres than in oxidizing ones. More distinct and stronger XRD peaks appeared only for the air-annealed sample in comparison to the H_2-treated and as-prepared ones. From EIS and DSC measurements, we confirm that H_2 can enable a higher crystallization temperature where the conductivity "bend-over" starts. Doping 5 mol% Al into $Na_2Si_2O_5$ also benefits the retention of the amorphous phase, thus the stability of conductivity. The amorphous phase of AL-$Na_2Si_2O_5$ did not change in either H_2 or in air at 500 °C, and the DSC analysis indicated a higher crystallization temperature than the AM-$Na_2Si_2O_5$. Raman spectroscopy only showed the features of tetrahedral structure for both AM/AL-$Na_2Si_2O_5$, but cannot discern the structural differences in reducing and oxidizing atmospheres. The multi-nucleus NMR revealed rich information in local environment of cations and anions in AM-$Na_2Si_2O_5$, in particular, the absence of protons in the material and Al-doping on *Si*-site forming sodium aluminosilicate.

Acknowledgment

This work is funded by the Advanced Research Projects Agency-Energy (ARPA-E), U.S. Department of Energy, under Award number DE-AR0000492 and the National Science Foundation under Award number 1508404. We would also like to thank Libin Lei for assisting the DSC measurements.

References

[1] C.E. Derrington, M. O'Keeffe, Nature Phys. Sci. 246 (1973) 44–46.
[2] G.A. Samara, J. Phys. Chem. Solids 40 (1979) 509–522.
[3] J. Oberschmidt, D. Lazarus, Phys. Rev. B 21 (1980) 2952–2961.
[4] C. Tubandt, E.Z. Lorenz, Phys. Chem. 24 (1914) 513–543.
[5] K. Funke, Prog. Solid State Chem. 11 (1976) 345–402.
[6] M. Tatsumisago, Y. Shinkuma, T. Minami, Nature 354 (1991) 217–218.
[7] A.V. Virkar, G.R. Miller, R.S. Gordon, J. Am. Ceram. Soc. 61 (1978) 250–252.
[8] G.E. Youngblood, G.R. Miller, R.S. Gordon, J.Am. Ceram. Soc. 61 (1978) 86–87.
[9] V. Thangadurai, H. Kaack, W.J.F. Weppner, J. Am. Ceram. Soc. 86 (2003) 437–440.
[10] V. Thangadurai, S. Adams, W.J.F. Weppner, Chem. Mater. 16 (2004) 2998–3006.
[11] J.-H. Park, J. Electrochem. Soc. 136 (1989) 2867–2876.
[12] X. Lei, Y. Jee, K. Huang, J. Mater, Chem. A 3 (2015) 19920–19927.
[13] J.R. Peet, C.M. Widdifield, D.C. Apperley, P. Hodgkinson, M.R. Johnson, I.R. Evans, Chem. Commun. 51 (2015) 17163–17165.
[14] Y. Jee, X. Zhao, K. Huang, Chem. Commun. 51 (2015) 9640–9642.
[15] Y. Jee, X. Zhao, X. Lei, K. Huang, J. Am. Ceram. Soc. 99 (2015) 324–331.
[16] M.G. Mortuza, R. Dupree, D. Holland, J. Mater. Sci. 33 (1998) 3737–3740.
[17] R. Pornprasertsuk, O. Kosasang, K. Somroop, M. Horprathum, P. Limnonthakul, P. Chindaudom, S. Jinawath, Solid State Sci. 13 (2011) 1429–1437.
[18] K.-Y. Park, T.-H. Lee, J.-T. Kim, N. Lee, Y. Seo, S.-J. Song, J.-Y. Park, J. Alloys, Compd. 585 (2014) 103–110.
[19] M.E. Fleet, G.S. Henderson, Phys. Chem. Miner. 24 (1997) 345–355.
[20] X. Ai, F. Deng, J. Dong, L. Chen, C. Ye, J. Phys. Chem. B 106 (2002) 9237–9244.
[21] A.K. Pant, Acta Cryst B24 (1968) 1077–1083.
[22] V. Kahlenberg, G. Dorsam, M. Wendschuh-Josties, R.X. Fischer, J. Solid State, Chemistry 146 (1999) 380–386.
[23] M.E. Fleet, J. Solid State, Chemistry 119 (1995) 400–404.
[24] P.F. McMillan, G.H. Wolf, in: J.F. Stebbins, P.F. McMillan, D.B. Dingwell (Eds.), Reviews in Mineralogy Vol. 32: Structure, Dynamics and Properties of Silicate Melts, Mineralogical Society of America, Chantilly 1995, pp. 247–316.
[25] B.O. Mysen, D. Virgo, I. Kushiro, Am. Mineral. 66 (1981) 678–701.
[26] P.-H. Chien, Y. Jee, C. Huang, R. Dervişoğlu, I. Hung, Z. Gan, K. Huang, Y.-Y. Hu, Chem. Sci. (2016), http://dx.doi.org/10.1039/C5SC04270D.
[27] X. Xue, J.F. Stebbins, Phys. Chem. Miner. 20 (1993) 297–307.
[28] H. Maekawa, P. Florian, D. Massiot, H. Kiyono, M. Nakamura, J. Phys. Chem. 100 (1996) 5525–5532.
[29] X. Xue, J.F. Stebbins, M. Kanzaki, Am. Mineral. 79 (1994) 31–42.
[30] X. Pardal, F. Brunet, T. Charpentier, I. Pochard, A. Nonat, Inorg. Chem. 51 (2012) 1827–1836.
[31] J.F. Stebbins, S.K. Lee, J.V. Oglesby, Am. Mineral. 84 (1999) 983–986.
[32] U.I. Chung, J.Y. Lee, J. Non-Cryst. Solids 110 (1989) 203–210.
[33] Y. Li, H. Ren, Y. Zhang, Z. Liu, H. Zhang, Int. J. Hydrogen Energ. 40 (2015) 7093–7102.